JOURNAL OF MATERIALS SCIENCE 9 (1974) 279–288

Recrystallization in internally oxidized Cu-Ag-Al alloys

O. K. CHOPRA, P. NIESSEN
Department of Mechanical Engineering, University of Waterloo, Waterloo, Ontario, Canada

The isothermal recrystallization kinetics of rolled Cu-Ag alloys containing up to 0.9 vol % alumina have been followed through hardness measurements; and nucleation rates have been obtained by X-ray back-reflection techniques. Electron microscopic studies have been carried out to characterize the as-deformed structures and the structural changes occurring during the annealing process. The recrystallization of the alloys was either accelerated or retarded as the alumina content increased. This effect has been found to depend both on the dispersion parameters and the degree of deformation. The recrystallization behaviour of these alloys is controlled primarily by the nucleation process. Nucleation occurred after an incubation period and involved the formation of subgrains from the cell structure and their subsequent growth to a viable size. The difficulty of the formation of viable nuclei has been attributed to the particle restraint on sub-boundary migration and to the lack of heavily distorted regions in the defect structure. The rate of nucleation was a function of time and found to depend on the dispersion, initial deformation and the temperature of anneal. The process of grain boundary migration during recrystallization was anisotropic.

1. Introduction

The strong influence of a finely dispersed stable phase on the recrystallization kinetics of deformed metals has been studied extensively in recent years [1-5]. Thin film transmission electron microscopy has been employed to study the process of annealing in terms of the nature and changes in the defect structure [6-10]. These observations showed that a dispersed phase can either accelerate or retard primary recrystallization, depending primarily on the spacing between particles.

Primary recrystallization involves the nucleation and growth of new grains and for a complete understanding of recrystallization it is desirable to know how these two mechanisms depend on the various material and process variables. Some investigations have shown that the observed recrystallization behaviour in dispersion hardened alloys, is largely determined by the influence of the dispersed phase on the rate of nucleation [1, 2]. Others have shown that the growth of new grains is retarded by the particles [11-13]. The results have generally been interpreted in terms of the particle restraint on mobile boundaries and sub-boundaries. However, very few studies have correlated the kinetic data and the microstructural observations for recrystallization.

This investigation was undertaken to study in detail the total recrystallization process of oxide dispersed alloys of copper, by direct measurements of nucleation rates and overall recrystallization kinetics and by electron microscopic observations of the defect structure produced after deformation and its subsequent annealing. The copper-alumina system was chosen for study because the alumina particles do not agglomerate or dissolve at high temperatures.

2. Experimental

2.1. Alloy preparation

Alloys of copper containing 0.04 at. % Ag and 0.0, 0.1, 0.25 and 0.5 at. % Al were used in this investigation. The silver was added to eliminate the unpredictable effect of residual impurities. It has been shown [14] that the addition of only 0.015 at. % Ag increases the recrystallization temperature of copper and eliminates the influence of the common impurities in copper.

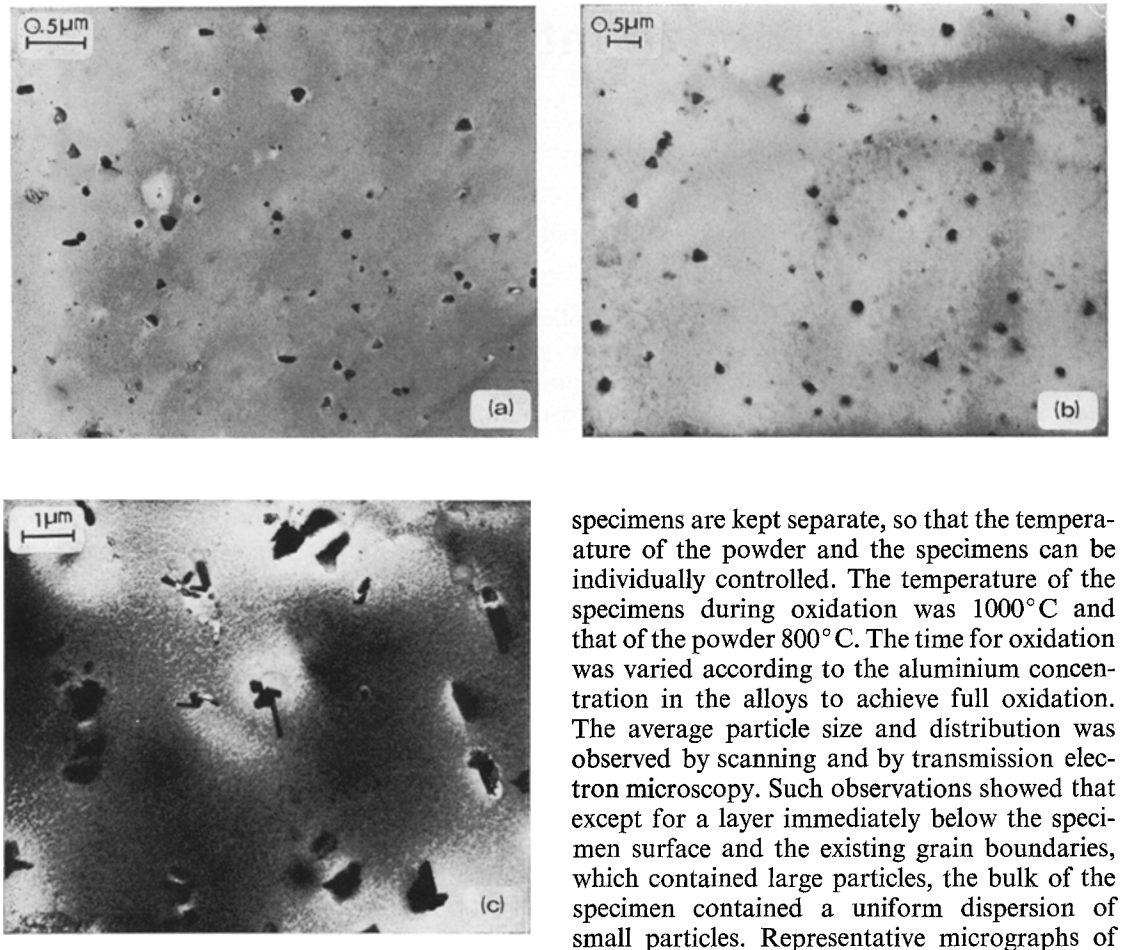

Figure 1 Microstructure of Cu-Ag-Al alloys after internal oxidation at 1000°C with the Cu-Cu_2O pack at 800°C. (a) 0.18 vol % Al_2O_3 (b) 0.45 vol % Al_2O_3 (c) 0.90 vol % Al_2O_3.

The alloys were prepared by melting appropriate amounts of OFHP copper and a master alloy of 5% Al in an induction furnace using a graphite crucible. The melt was covered with charcoal powder and bottom poured into a split graphite mould. The as-cast bars were machined and rolled to 3.5 mm thickness. Specimens of appropriate size were cut from the rolled strip and annealed at 800°C for 24 h under an argon atmosphere and furnace cooled to room temperature.

A dispersion of small oxide particles was obtained in the specimens by internal oxidation using the modified Rhines method described by Ramaswami and Kupcis [15]. In this method, the copper-cuprous oxide powder and the specimens are kept separate, so that the temperature of the powder and the specimens can be individually controlled. The temperature of the specimens during oxidation was 1000°C and that of the powder 800°C. The time for oxidation was varied according to the aluminium concentration in the alloys to achieve full oxidation. The average particle size and distribution was observed by scanning and by transmission electron microscopy. Such observations showed that except for a layer immediately below the specimen surface and the existing grain boundaries, which contained large particles, the bulk of the specimen contained a uniform dispersion of small particles. Representative micrographs of the dispersion in the different oxidized alloys are shown in Fig. 1. In order to eliminate the surface effects, a layer of 0.2 mm of the specimen surface was removed prior to the final deformation.

2.2. Recrystallization

The recrystallization process was studied by conducting isothermal recrystallization experiments and measuring the fraction recrystallized and nucleation rates. The structures of the deformed and annealed specimens at various stages of recrystallization were examined by optical and electron microscopy. All specimens were given a final deformation of 70% (final thickness of the specimens approximately 1 mm) by rolling at room temperature. In addition, the Cu-Ag-0.18 vol % Al_2O_3 alloy was also deformed 50% by rolling to study the effect of the initial deformation on the recrystallization process. Annealing was carried out in a binary nitrate salt bath. The temperature of the bath was controlled to within ± 1°C.

The fraction recrystallized was followed by hardness measurements. A Rockwell superficial hardness tester was used for this purpose. The nucleation rates were obtained by taking X-ray back-reflection patterns from the specimens which were annealed isothermally for different times and counting the number of reflections on a particular Debeye ring. The number of reflections is proportional to the number of grains present at any time of the recrystallization process. The specimens were traversed back and forth over 1 cm to gather reflections from a large area of the specimen. In order to establish the homogeneity of nucleation within the bulk of the specimens, back reflection patterns were obtained from several areas on the specimen surface, at various depths below the surface and on the cross-sections along and transverse to the rolling direction. No difference was observed in the average value of the number of reflections from the different regions of a specimen. Subsequently, patterns were obtained from the longitudinal cross-section of the specimens of the various alloys. Several portions were traversed for each specimen to obtain an average value for the number of grains.

Thin foils were prepared from the bulk material for transmission electron microscopy. They were first thinned mechanically and then chemically to a thickness of 0.07 mm. The final thinning was carried out by jet polishing using an electrolyte of 30% orthophosphoric acid.

2.3. Particle size and spacing

The average particle radius and interparticle spacing was determined by transmission electron microscopy using the method described by Lewis and Martin [16]. The number of particles in a known volume of thin foil observed by transmission electron microscopy was calculated by counting particles in several randomly positioned regions of the foils for each alloy. The foil thickness was measured and the volume fraction of the dispersed phase was calculated knowing the composition of the alloy and assuming complete oxidation of the aluminium. The average sizes and spacings obtained for two of the oxidized Cu-Ag-Al alloys are given in Table I. These values could not be determined for the alloy containing 0.9 vol % alumina because of difficulties in preparing thin foils of this alloy.

3. Results

3.1. Recrystallization kinetics

The recrystallization curves as a function of the decrease in Rockwell hardness after isothermal annealing at different temperatures for various times were obtained for all the alloys. An example of these softening curves is shown in Fig. 2a. The Rockwell hardness numbers were then converted to Vickers hardness numbers as

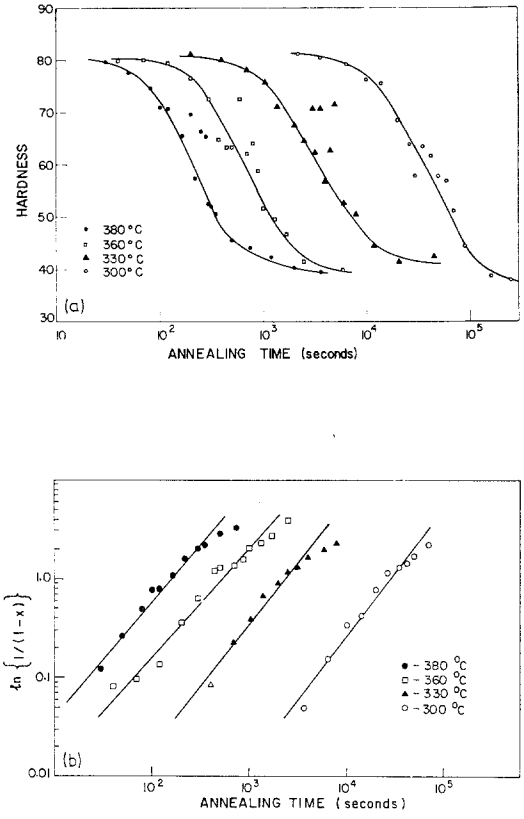

Figure 2 (a) Isothermal recrystallization curves of hardness versus annealing time for Cu-0.04 at. % Ag-0.45 vol % Al_2O_3 after 70% rolling. (b) Plot of the values of the fraction recrystallized "x" versus time, obtained from data in (a).

TABLE I Particle sizes and interparticle spacings

Alloy	Vol % alumina	Particle radius (Å)	Interparticle spacing (μm)
Cu-0.04 at. % Ag-0.1 at. % Al	0.18	175	0.56
Cu-0.04 at. % Ag-0.25 at. % Al	0.45	290	0.58

described in a former study [17] and the values of the fraction recrystallized obtained from the decrease in VHN as a function of time. It has been shown [17] that the decrease in VHN is representative of the volume fraction recrystallized.

From these recrystallization curves, the time for 50% recrystallization was determined. The values are given in Table II and their logarithms are plotted against the inverse temperature in Fig. 3. It is seen that after 70% rolling, the influence of increasing volume fraction of alumina, as compared to the oxide-free alloy, can either accelerate or retard the recrystallization process. For example, for the same temperature, recrystallization is faster in 0.18 vol % alumina whereas it is slower in 0.45 vol % alumina alloy. The initial amount of deformation is also an important parameter. For the same volume fraction of alumina and annealing temperature recrystallization is accelerated in the specimens which were rolled 70%, whereas it is retarded in the specimens which were rolled 50%.

These isothermal recrystallization results were compared with the Avrami equation

$$x = 1 - \exp(-kt^n)$$

where x is the volume fraction recrystallized, t is the annealing time and k and n are constants. Plots of $\ln \ln\{1/(1-x)\}$ versus $\ln t$ were produced. Fig. 2b shows the plots for one of the alloys. The straight lines resulting from the plot show that the recrystallization data do obey this equation. However, a deviation from linearity occurs when the fraction recrystallized exceeds 0.7. The slopes of the plots yield the values of the time exponent n. The values of n were obtained using a least square analysis and considering only those experimental points which corresponded to recrystallized fractions between the range of 0.05 to 0.7. These values are listed in Table II. It is seen that for the oxidized alloys the values of n are generally low and are independent of the temperature of anneal or the volume fraction of oxide.

TABLE II Kinetics of recrystallization

Vol % alumina	Deformation (%)	Temperature (°C)	Time for 50% recrystallization (sec)	Time exponent n	Activation energy (kcal (g. at.)$^{-1}$)	
					Overall recrystallization	Nucleation process
0.0*	50	360	2100	1.46		
0.0	70	300	9000	1.14		
		330	1050	1.04	46.8	
		360	190	1.23		
0.18	50	360	8500	0.90		
		380	2000	0.91	49.0	48.2
		400	620	0.94		
		425	210	1.07		
0.18	70	290	13500	1.13		
		310	3600	1.28	48.5	47.2
		330	780	1.09		
		360	130	1.18		
0.45	70	300	19000	1.21		
		330	2400	1.06	47.6	46.8
		360	400	1.06		
		380	120	1.16		
0.90	70	300	11000	1.14		
		330	1300	1.01	47.1	
		360	210	1.28		
		380	75	1.13		

*Reference 17.

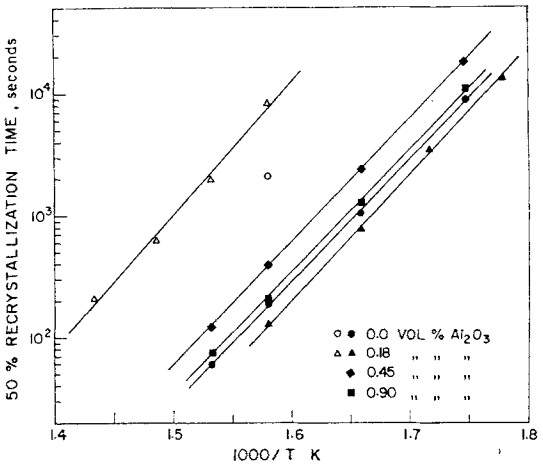

Figure 3 Plot of the values of the time for 50% recrystallization versus inverse absolute temperature of anneal. Open points rolled 50% and filled points rolled 70%.

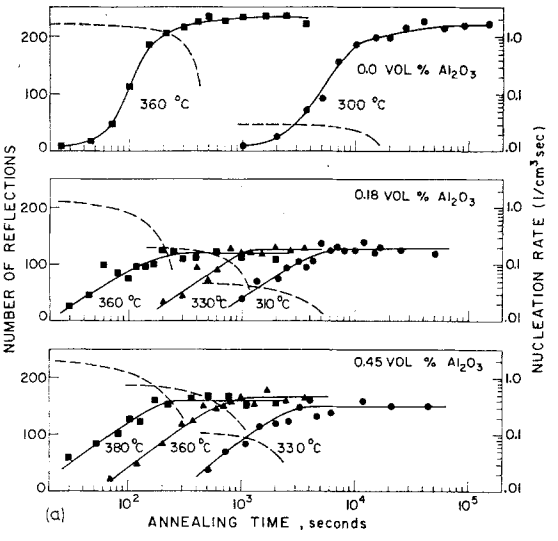

Considering the temperature dependence of recrystallization, the activation energies for the overall recrystallization process were obtained, Fig. 3. These values are also presented in Table II. There is no apparent change in the activation energy due to the presence of alumina or with a change in volume fraction of alumina.

3.2. Nucleation rates

The number of nuclei formed during recrystallization was determined as a function of the number of reflections on the Debye rings obtained by X-ray back-reflection from a fixed area of the specimen surface. These curves are shown as continuous lines in Fig. 4a for alloys annealed after 70% rolling. The slope of these curves at a particular time gives the instantaneous nucleation rate per unit volume of the specimen. The true nucleation rates, i.e. the rate of nucleation in the unrecrystallized volume, were obtained using the instantaneous nucleation rates and the results of the overall recrystallization kinetic. They are shown as dotted lines. Corresponding curves obtained for the Cu-Ag-0.18 vol % Al_2O_3 alloy rolled 50% are shown in Fig. 4b.

These curves show that the nucleation rates are not constant but change with time depending on the alloy composition, initial deformation and the temperature of anneal. In general, the nucleation rates increase with annealing temperature and initial deformation, other experimental variables being constant. For a fixed temperature

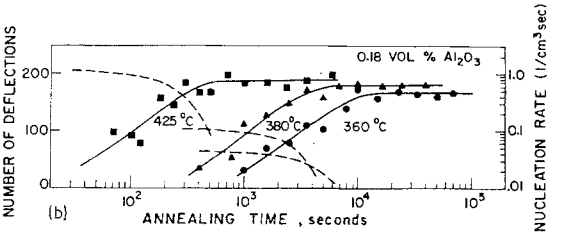

Figure 4 (a) Number of reflections and instantaneous nucleation rates versus annealing time from isothermally annealed specimens of Cu-0.04 at. % Ag-Al_2O_3 alloys rolled 70%. (b) Number of reflections and instantaneous nucleation rates versus annealing time from isothermally annealed specimens of Cu-0.04 at.% Ag-0.18 vol% Al_2O_3 alloys rolled 50%.

and deformation the nucleation rates for the oxide-free alloy and the 0.18 vol % alumina alloys are essentially the same, but the rates are lower for the 0.45 vol % alumina alloys. Comparison of these curves with the isothermal recrystallization curves show that nucleation occurs throughout the recrystallization process. The nucleation rates are relatively constant initially and decrease rapidly after approximately 50% of the volume has recrystallized.

From the temperature dependence of the nucleation rate expressed as

$$\dot{N} = \dot{N}_0 \exp(-Q_N/RT)$$

the activation energy Q_N for the nucleation process was obtained. The nucleation rates observed when 10% of the volume has recrystal-

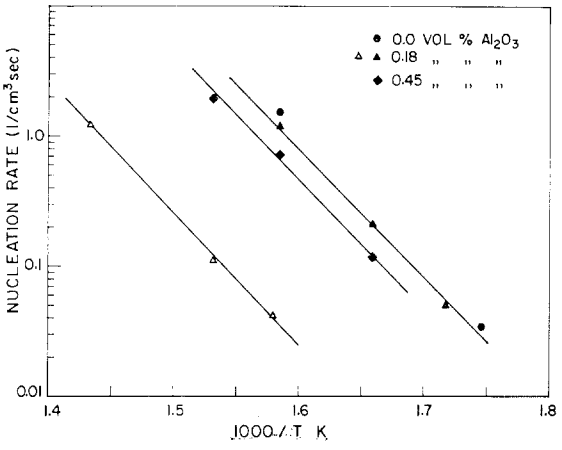

Figure 5 Plot of the rate of nucleation versus inverse absolute temperature of anneal. Open points rolled 50% and filled points rolled 70%.

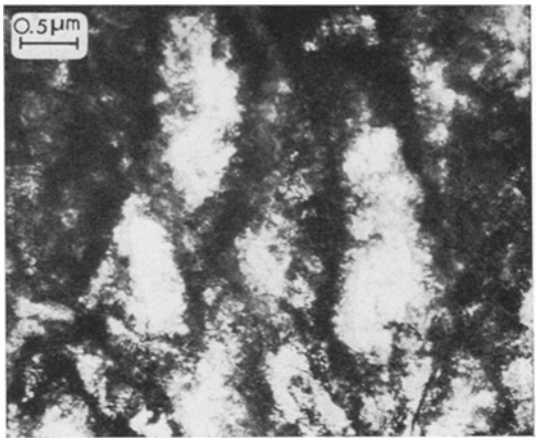

Figure 6 Microstructures after 70% rolling of Cu-0.04 at. % Ag-0.45 vol % Al_2O_3 alloy.

lized, are plotted against inverse absolute temperature in Fig. 5. These values are listed in Table II. There is no apparent difference between the activation energy for nucleation in the oxide-free and the oxidized alloys.

3.3. Deformation structure

The structure observed after deformation of the alloys containing 0.18 and 0.45 vol % alumina showed the formation of a diffuse but definite cell structure after 30% rolling. Upon further deformation, the cells became elongated but the cell walls remained diffuse even after 70% rolling. Most of the oxide particles were seen to be associated with the dislocations within the cell walls. The average cell size in both the alloys was found to be the same and was approximately 0.6 μm. In view of the fact that the average interparticle spacing in both these alloys is also of the same order, it would appear that the particle spacing controls the cell size obtained during deformation of these alloys. A typical structure observed after 70% rolling in the alloy containing 0.45 vol % alumina is shown in Fig. 6

3.4. Structural changes

The microstructural changes which occur during the early stages of annealing of the oxidized alloys show the gradual recovery of the deformation structure to produce nuclei of strain-free grains. The structures observed in the specimens depended on the time and temperature of anneal. In all cases, nuclei bounded by high angle boundaries separating the recrystallized and the deformed regions were observed only after a certain time or an incubation period. The appearance of the nuclei coincided with a marked decrease in hardness. The incubation period was characterized by rearrangement and modification of the deformed structure. No difference in the mechanism of formation of nuclei was observed among the different oxidized alloys. In all cases, subgrains were observed to form by considerable rearrangement of the existing cell structure, as seen in Fig. 7. Moiré fringes and extinction contours can be observed along the sub-boundaries and sharp interface. Arrays of parallel dislocations can be seen in many regions. The sub-boundaries defining the strain-free region A appear to be held up by the oxide particles.

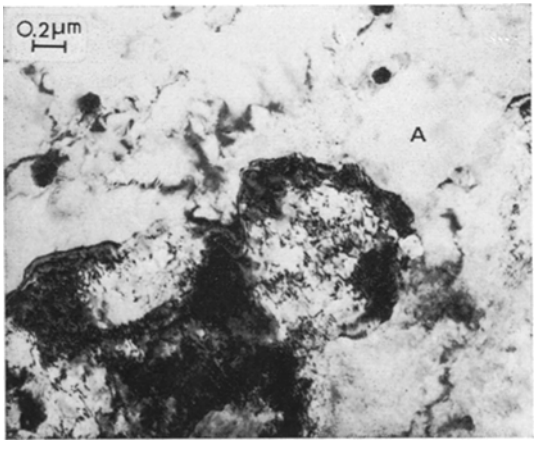

Figure 7 Cu-0.04 at. % Ag-0.18 vol % Al_2O_3 annealed for 200 sec at 330°C after 70% rolling.

Figure 8 Cu-0.04 at. % Ag-0.18 vol % Al_2O_3 annealed for 4000 sec at 290° C after 70% rolling. Arrows show the regions where the boundary is pinned due to the oxide particles.

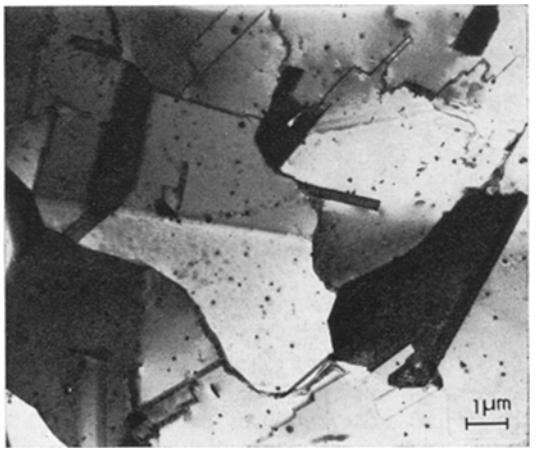

Figure 9 Cu-0.04 at. % Ag-0.18 vol % Al_2O_3 after complete recrystallization.

Observations of the specimens in the later stages of recrystallization show these new grains at various stages of growth, Figs. 8 and 9. The boundaries migrate at the expense of the deformed matrix. The presence of the oxide particles impedes the process of boundary migration. A large number of bulges can be seen along the migrating boundary at low magnification, Figs. 10a and b, indicating the pinning effect of the particles. The main characteristic of the recrystallized grains is the presence of a considerable number of annealing twins even during the early stages of growth, Figs. 8 and 10b. Most of the recrystallized grains are elongated

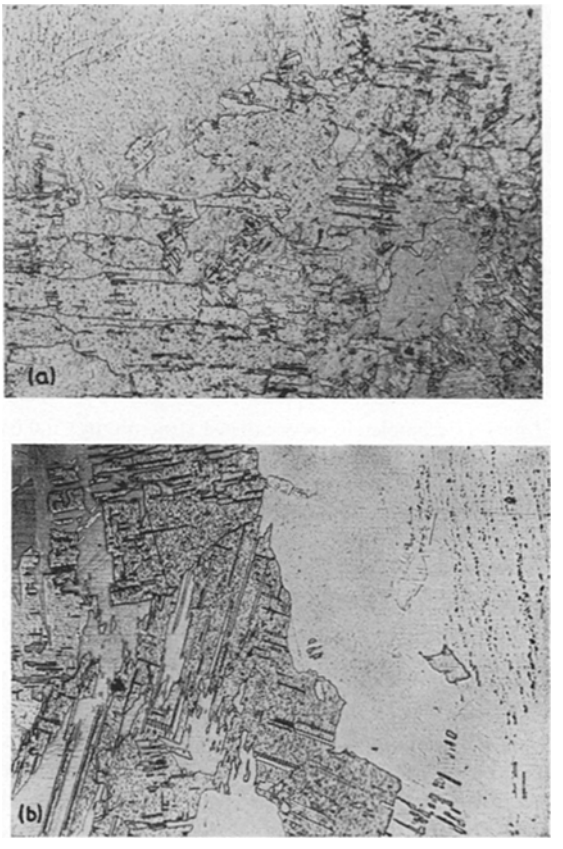

Figure 10 (a) Cu-0.04 at. % Ag-0.45 vol % Al_2O_3 annealed for 700 sec at 330° C after 70% rolling (× 140). (b) Cu-0.04 at. % Ag-0.18 vol % Al_2O_3 annealed for 200 sec at 360° C after 70% rolling (× 140).

and contain parallel twins. Also, it is seen that recrystallization is almost complete in some of the existing grains while neighbouring grains show no sign of start of recrystallization. New grains are observed to form predominantly within the existing grains, however, in some cases it is difficult to say whether they formed along a pre-existing boundary or in the deformed matrix adjacent to the boundary.

A typical structure observed after complete recrystallization of these alloys is shown in Fig. 11. The number of twins observed in these structures is considerably less than that during the early stages of recrystallization. At this stage, the grain boundaries are smooth although a very non-uniform grain size is observed.

4. Discussion

The isothermal recrystallization curves are of the standard sigmoidal form and follow the

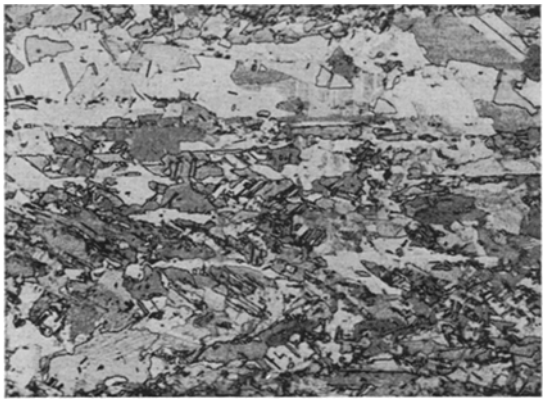

Figure 11 Completely recrystallized structure in Cu-0.04 at. % Ag-0.45 vol % Al_2O_3 (× 88).

Avrami equation. They show that the recrystallization behaviour of the oxidized alloys, as compared to the oxide-free alloy, can either be accelerated or retarded depending on the dispersion parameters and the degree of initial deformation. Comparing Figs. 3 and 5, it is seen that the nucleation rates also follow this rate behaviour. The nucleation rates are high for the alloy in which recrystallization is accelerated and are low for the alloy in which it is retarded, with the exception of the 0.18 vol % alumina alloy annealed after 70% rolling. Although there is little or no change in the nucleation rate between this alloy and the oxide-free alloy, the overall recrystallization is slightly faster in the oxidized alloy. These observations indicate that the overall recrystallization behaviour of the oxidized alloys is controlled essentially by the rate of nucleation, i.e. the rate at which viable nuclei are formed.

It should be pointed out that the accuracy of the measurements of nucleation rates depends on the degree to which the nuclei can be resolved by the experimental technique. It could, therefore, be argued that the measured values of nucleation rates also reflect the initial rate of grain-boundary migration of viable nuclei. Consequently, the observed variation of nucleation rates arises due to an inhibition of the growth process preventing the recrystallized grains from attaining a detectable size. However, this does not seem to be true for these studies. Electron microscopic observations of recrystallized grains or subgrains coincided with the appearance of reflections on the X-ray back-reflection pattern and a decrease in hardness values.

4.1. Nucleation

From Fig. 5 it is seen that the activation energy for nucleation is the same for all the alloys. This would indicate that the basic mechanism of nucleation is the same for these alloys and the difference in the nucleation rates is due to a change in the pre-exponential term of the rate equation given in the previous section. This term includes the effective driving force for nucleation.

The micrographs show that nucleation occurs primarily in the matrix and involves the gradual healing of the as-deformed structure to produce sharp well-defined subgrains having the thermodynamic ability to grow. The subgrains do not form by the recovery of the existing cell structure but require considerable rearrangement and long range motion of dislocations to produce new strain free regions. Nucleation by the bulging of the existing grain boundaries was not observed in these alloys. The presence of a great number of particles along the existing boundaries would inhibit such a mechanism of nucleation.

It has been shown that during deformation of dispersion-hardened alloys, slip generally occurs on various slip systems and that long range motion of dislocations is prevented by the presence of particles, resulting in a complex distribution of dislocations and the formation of a very diffuse cell structure [16, 18]. However, the physical size and shape of the particles also influence the resulting deformation structure [10]. Dislocation interactions with large particles lead to greater misorientations or rotations of the lattice adjacent to the particles, specially after severe deformation. These regions act as potential sites for nucleation.

In view of the foregoing, it is seen that both the initial deformation and the dispersion parameters can alter the nature of the deformation structure so as to accelerate or retard the nucleation rates as compared to the oxide-free alloy. In other words, the effective driving force and hence the rate of nucleation would be controlled by both these factors. Formulation of nuclei should be more difficult after lower initial deformation because of lack of regions having large misorientations as, in fact observed in the case of 0.18 vol % alumina, Figs. 4a and b.

For a given amount of initial deformation, the rate of formation of viable nuclei would also be controlled by the direct particle restraint on

the migrating sub-boundaries. The ability of a given volume fraction of dispersed phase to slow a migrating boundary is a function of the fineness of dispersion and can be expressed by the Zener relation [19]. This relation predicts that growth rates are retarded by a factor f/r, where f is the volume fraction of dispersed phase and r the particle radius. From Table I it is seen that while the interparticle spacing is approximately the same for the alloys containing 0.18 and 0.45 vol % alumina, f/r is greater for the 0.45 vol % alumina alloy. Consequently, the effective driving force would be reduced and, hence, formation of viable nuclei should be retarded in this alloy. Fig. 4a shows that the nucleation rate is indeed lower in this alloy.

The reduction in nucleation rate with time occurs because the number of preferred sites for nucleation become exhausted, and recovery reduces the driving force for sub-boundary migrating so that the Zener drag becomes more pronounced.

4.2. Growth

Growth of the new grains involves the migration of high angle boundaries. A very inhomogeneous recrystallization behaviour is observed in this alloy; some of the existing grains show no sign of recrystallization, Fig. 10a. The reluctance of the recrystallized grains to grow into the adjacent matrix indicates a strong dependence of grain-boundary migration on the nature of the defect structure. This dependence is reflected in the values of the time exponent n obtained from the isothermal recrystallization kinetics. The very low values of n indicate a very anisotropic behaviour of grain-boundary migration [20]. It is believed that this anisotropy is caused by the difference in the recrystallization behaviour of the originally existing grains and their crystallographic orientation with respect to the rolling plane [21].

In this connection, it is interesting to note the extremely high twinning frequency observed in these alloys, Figure 10b. A very non-uniform grain size is seen and the grains contain a large number of parallel twins. These observations imply a preferred direction of growth. For a number of microscopic observations, e.g. Fig. 8, it appears that twins are formed in order for the boundary to maintain a high mobility of individual segments.

5. Conclusions

The isothermal recrystallization behaviour of internally oxidized Cu-Ag-Al alloys has been shown to be a function of the deformation structure and the dispersion parameters. The overall recrystallization rate can be expressed by the Avrami equation and is controlled basically by the nucleation process.

Nucleation occurs primarily by the gradual healing of the heavily distorted regions to produce subgrains. There is an incubation period before viable nuclei can be produced. The rates of nucleation change with time and depend both on the dispersion parameters and the degree of initial deformation.

The process of grain-boundary migration shows an anisotropic behaviour. The formation of annealing twins plays a large role in maintaining high grain-boundary mobilities.

Acknowledgement

This research was supported by the National Research Council of Canada.

References

1. R. D. DOHERTY and J. W. MARTIN, *Trans. ASM* **57** (1964) 874.
2. P. R. MOULD and P. COTTERILL, *J. Mater. Sci.* **2** (1967) 241.
3. A. GATTI and R. FULLMAN, *Trans. Met. Soc. AIME* **215** (1959) 762.
4. O. PRESTON and N. J. GRANT, *ibid* **221** (1961) 164.
5. F. J. HUMPHREYS and J. W. MARTIN, *Acta Metallurgica* **14** (1966) 775.
6. J. L. BRIMHALL, M. J. KLEIN and R. A. HUGGINS, *ibid* **14** (1966) 459.
7. D. NOBILI and T. DE MARIA, *J. Nuclear. Mater.* **17** (1965) 5.
8. G. F. MISSIROLI, D. NOBILI and R. ZIGNANI, *ibid* **21** (1967) 199.
9. F. J. HUMPHREYS and J. W. MARTIN, *Phil. Mag.* **17** (1968) 365.
10. T. C. ROLLASON and J. W. MARTIN, *J. Mater. Sci.* **5** (1970) 127.
11. D. L. WOOD, *Trans. Met. Soc. AIME* **215** (1959) 925.
12. A. DESALVO and D. NOBILI, *J. Mater. Sci.* **3** (1968) 1.
13. D. NOBILI, F. MEZZETTI and E. S. DEMARIA, *ibid* **3** (1968) 282.
14. W. DAHL and J. GEISSLER, *Z. Metallk.* **51** (1960) 421.
15. O. A. KUPCIS and B. RAMASWAMI, *Mat. Sci. Eng.* **5** (1969/70) 43.
16. M. H. LEWIS and J. W. MARTIN, *Acta Metallurgica* **11** (1963) 1207.
17. O. K. CHOPRA and P. NIESSEN, *J. Mater. Sci.* **8** (1973) 93.
18. J. L. BRIMHALL and R. A. HUGGINS, *Trans. Met. Soc. AIME* **233** (1965) 1076.

19. C. S. SMITH, *ibid* **175** (1948) 15.
20. J. W. CHRISTIAN, "Physical Metallurgy" (edited by R. W. Cahn) (North-Holland, Amsterdam, 1970) p. 471.
21. W. R. HIBBARD, JUN. and W. R. TULLY, *Trans. Met. Soc. AIME* **221** (1961) 336.

Received 13 June and accepted 24 August 1973.